Journal of Materials Chemistry A

Accepted Manuscript

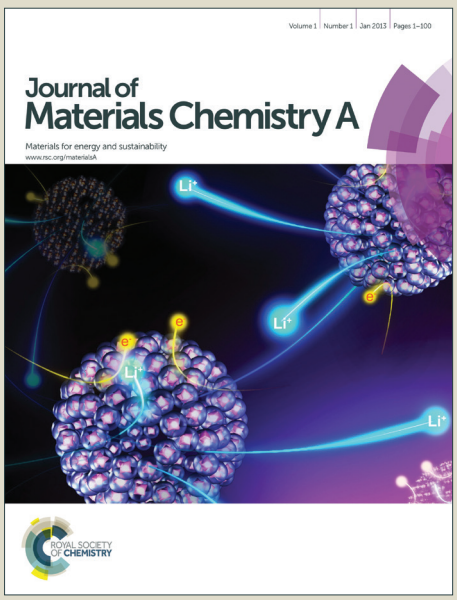

ROYAL SOCIETY OF CHEMISTRY

www.rsc.org/materialsA

Journal Name

ARTICLE

Graphene-Wrapped Mesoporous $MnCO_3$ Single Crystals Synthesized from Dynamic Floating Electrodeposition Method for High Performance Lithium-ion Storage

Received 00th January 20xx,
Accepted 00th January 20xx

DOI: 10.1039/x0xx00000x

www.rsc.org/

Mingwen Gao,[a] Xinwei Cui,*[b] Renfei Wang,[b] Tianfei Wang,[b] and Weixing Chen,*[a,b]

A unique structure of graphene-wrapped mesoporous single crystals (MSCs) is successfully applied on low-cost $MnCO_3$ for lithium-ion batteries (LIBs). In a departure from previous high-temperature (>500°C) synthesis approaches for MSCs, we develop a simple, low-temperature (70°C) and template-free method, referrers to as dynamic floating electrodeposition (DFE), to fabricate graphene-wrapped $MnCO_3$ MSCs. In DFE method, we achieve the reduction of GOs to RGOs, the deposition of $MnCO_3$ MSCs on graphene, and graphene-wrapped morphology, all three goals in one electrochemical process. The resulting submicron, graphene-wrapped $MnCO_3$ MSCs reaches a high reversible capacity of 900 mAh g^{-1} after the initial cycle and delivered over 1,000 mAh g^{-1} after 130 cycles. The reversible capacity is also kept at this high level for more than 400 cycles and maintained 422 mAh g^{-1} at a high rate of 5,000 mA g^{-1}. It is the first time that this high performance is achieved on $MnCO_3$ for lithium-ion storage. Furthermore, this superior electrochemical performance is found to be highly related to the designed structure, graphene-wrapped MSCs, of $MnCO_3$.

Introduction

Electrochemically active transition metal oxides (MO_x), such as FeO_x,[1,2] CoO_x,[3,4] SnO_2,[5-7] and MnO_x,[8-12] have been widely used as promising candidates for anode materials in lithium-ion batteries (LIBs). Besides these metal oxides, $MnCO_3$ is naturally abundant, environmentally friendly, and often used as a precursor for MnO_2 synthesis;[13-15] and hence, its cost is even lower than MnO_2 and most of the transition-metal oxides. However, very few researches have been reported to use $MnCO_3$ directly as electrochemically active materials. Yan et al. has reported a reversible capacity of 750 mAh g^{-1} for $MnCO_3$ when used as anodes in LIBs, which is comparable to that reported for MnO_2 (495 mAh g^{-1} ~900 mAh g^{-1}).[8-10,15] However, its capacity quickly drops down to 200 mAh g^{-1} after 100 cycles, which is due to the intrinsic low electrical conductivity and the compact morphology of hydrothermal $MnCO_3$ micro-particles.[15,16] Poizot et al. also found that the electrochemical performance of metal-oxide particles was affected by their morphology, e.g., the particle size and crystal structure of metal oxides.[17] Therefore, the electrical conductivity and the morphology of $MnCO_3$ need to be optimized for lithium-ion storage.

Mesoporous single crystals (MSCs) promise excellent features for energy storage, such as high-rate lithiation/delithiation capability, long-range electronic connectivity, and high structural integrity.[18-21] However, the application of MSCs was limited by their complex and high temperature (>500°C) synthesizing processes, involving template planting and removing.[18,22-24] In addition, graphene wrapped structure offers a highly conductive shell and provides additional protection to the wrapped particles during cycling.[10,25] To the best of our knowledge, their combination, the graphene-wrapped MSC structure, although highly demanded for energy storage, hasn't been reported so far.

Here, we designed a unique morphology of graphene-wrapped MSC for $MnCO_3$ and directly used it as anode materials in LIBs. In a departure from previous high-temperature synthesis approaches, we developed a simple, low-temperature (70°C) and template-free method, referred to as dynamic floating electrodeposition (DFE) (Fig. 1a), to fabricate graphene-wrapped $MnCO_3$ MSCs. Instead of only reducing GOs to RGOs in the electrochemical cell that has been reported by previous researchers,[26-28] we, for the first time, achieved the reduction of GOs to RGOs, the deposition of $MnCO_3$ MSCs on graphene, and graphene-wrapped morphology, all three goals in one electrochemical process. The resulting submicron, graphene-wrapped $MnCO_3$ MSCs reached a high reversible capacity of 900 mAh g^{-1} after the initial cycle and delivered over 1,000 mA g^{-1} after 130 cycles. Furthermore, the reversible capacity kept at this high level for more than 400 cycles and maintained 422 mAh g^{-1} at a high rate of 5,000 mA g^{-1}, demonstrating their great potential to be used as anodes in LIBs. It is also the first time that this

[a] Department of Chemical and Materials Engineering, University of Alberta, Edmonton, Alberta, Canada T6G 2G6 E-mail: weixing.chen@ualberta.ca
[b] AdvEn Solutions Inc. 3231 Tredger Close, Edmonton, Alberta, Canada, T6R 3T6 E-mail: xinwei.cui@adven-solution.com
Electronic Supplementary Information (ESI) available: [details of any supplementary information available should be included here]. See DOI: 10.1039/x0xx00000x

high performance has been achieved on $MnCO_3$ for lithium-ion storage. The structural design of the active materials, the DFE synthesis method, and the high performance for lithium-ion storage provided in this work may point out new directions in developing high performance energy storage systems.

Experimental

Material synthesis

GO preparation: The graphite oxide was synthesized from natural graphite powders (MTI Corporation) based on a modified Hummers method.[29,30] The exfoliation of graphite oxide to GO was achieved by sonication for 2 hours (Branson 2510, 1000 W, 20% amplitude), and then, GOs were filtered and rinsed with deionized water. Finally, a homogeneous GO in deionized water solution (2.0 mg mL^{-1}) was obtained and used for electrodeposition.

Synthesis of graphene-wrapped $MnCO_3$ MSCs by DFE method: The dynamic floating electrodeposition was carried out by Gamry PC4/750 potentiostat/galvanostat in a three-electrode cell configuration under galvanostatic control of the current density at 30 mA cm^{-2}, where Ag/AgCl was used as the reference electrode. The cathodic electrode was ferritic stainless steel substrates with dimensions of 20 mm× 10 mm × 1 mm, and the anodic electrode was a 52 mesh woven platinum sheet with dimensions of 20 mm× 10 mm. The cathodic and anodic electrodes were set in vertical position opposite to each other with a distance of 10 cm. The plating solution used was 0.3 M sodium citrated and 0.3 M $MnSO_4$ with the pH value adjusted to be 6.7~7.0. 20 mL GO (2.0 mg mL^{-1}) solution was then dispersed into 500 mL plating solution and agitated with Teflon-coated stirring bar at a speed of 700 rpm. During the electrodeposition, the temperature of the plating solution was controlled to be at 70°C. After electrodeposition for 4 hours, graphene-wrapped $MnCO_3$ MSCs were filtered from the plating solution, and rinsed with deionized water before freeze-dried (Savant supermodulyo freeze dryer, Thermo Electron Corporation) for over 10 hours.

Synthesis of nanocrystalline $MnCO_3$-RGO (nc-$MnCO_3$-RGO): Nanocrystalline $MnCO_3$ was synthesized by a hydrothermal method.[15] 0.474g $KMnO_4$, 0.595g glucose and 0.15g potassium sodium tartrate were dissolved in 50 mL of deionized water, which was then mixed to form a homogeneous solution by constant magnetic stirring. The resulting mixture was sealed into Teflon-lined autoclaves (60 mL) and heated at 160°C for 6 h. The final products of nanocrystalline $MnCO_3$ were then collected and washed with deionized water and absolute alcohol several times before vacuum dried. RGOs were reduced from GOs by refluxing with 0.8 g of glucose and 0.76 mL of ammonia solution (25 wt%) at 95°C for 1h. Nanocrystalline $MnCO_3$ particles were then homogeneously mixed with RGOs in deionized water with the weight ratio of 9:1 to form nc-$MnCO_3$-RGO, followed by freeze drying.

Synthesis of MnO_2 nanoflakes-RGO (nano-MnO_2-RGO): nano-MnO_2-RGO was prepared according to a two-step chemical method reported previously.[33] In brief, 0.23g of $KMnO_4$ was slowly added to 10 mL of the homogeneous GO/$MnSO_4$ solution, and the mixture was refluxed at 80°C for 2 hours for the fabrication of GO/MnO_2 composites. In the second step, the resulting GO/MnO_2 composites were refluxed with 0.8 g of glucose and 0.76 mL of ammonia solution (25 wt%) at 95°C for 1 h for the reduction of GO. The resulting stable black dispersion was centrifuged and washed with deionized water, which was followed by freeze drying to obtain nano-MnO_2- RGO.

Characterization

The morphology and structure of graphene-wrapped $MnCO_3$ MSCs, nc-$MnCO_3$-RGO and nano-MnO_2-RGO were analyzed by scanning electron microscopy (SEM, Hitachi S-5500, Hitachi S-4800, and Zeiss EVO SEM equipped with a Bruker Silicon Drift Detector for Energy Dispersive X-Ray analysis) and transmission electron microscopy (TEM, JEOL JEM-2100 with LaB6 cathode, 200 kV and JEOL 2010 attached with 4pi EDXS system). X-ray photoelectron spectroscopy (XPS) was carried out using a Kratos AXIS Ultra-x-ray photoelectron spectrometer. X-ray Diffraction (XRD) analyses were conducted on a Siemens D5000 X-ray diffractometer with Cu Kα as the radiation source (λ= 1.5418 A). Thermogravimetric analysis (TGA) was carried out (TA instruments, Q500) with a heating rate of 10°C min^{-1}.

Electrochemical measurement

The electrochemical experiments were performance using 2032-type coin cells. To prepare working electrodes, graphene-wrapped $MnCO_3$ MSCs, Super-C65 carbon black, and polyvinylidene fluoride with mass ratio 90:6:4 were mixed homogeneously in N-methyl pyrrolidone (NMP). The same ratio was used for making nc-$MnCO_3$-RGO and nano-MnO_2-RGO electrodes. The obtained slurry was pasted onto Cu foils, vacuum dried at 120°C overnight, and pressed. The total loading mass of the material on Cu foil was then determined to be ~2 mg cm^{-2} for all three composite materials. After cutting into a round disk with a diameter of 1.5 cm, the electrodes were assembled in an Argon-filled glove box, using the electrolyte of 1M LiPF6 in ethylene carbonate/diethyl carbonate/dimethyl carbonate (EC/DEC/DMC, vol 1:1:1) (MTI Corporation), 2 pieces of separator (Celgard 2500), and a pure lithium metal foil (MTI Corporation) as a counter electrode. The galvanostatic charge/discharge tests, cyclic voltammetry (CV) tests and cycle performance tests were carried out at 22 $\pm$ 1°C using a 1470E multi potentiostat/celltest system (Solartron).

Results and discussion

Dynamic flowing electrodeposition

The detailed DFE process to fabricate graphene-wrapped $MnCO_3$ MSCs is schematically shown in Fig. 1a. GOs were first

prepared from expandable graphite by modified Hummers method[29,30] and well dispersed in the aqueous electroplating bath of 0.3 M Na_3Cit and 0.3 M $MnSO_4$ at pH ~7.0 by magnetic stirring. The well dispersed GO suspension was formed due to a large amount of oxygenated groups bonded on the surface of GOs.[28] The anode was Pt mesh, the cathode used was stainless steel plate and the bath temperature was set to 70°C.

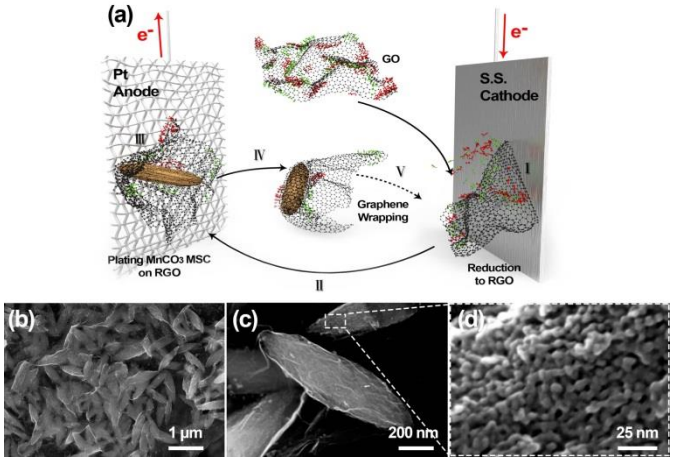

Fig. 1 (a) A schematic illustration of the dynamic floating electrodeposition method. SEM images of (b) the novel composite, (c) the graphene wrapping structure, and (d) the mesoporous structure.

During the electrodeposition, the floating GOs were the true electrodes and the whole process was dynamic. (I) When floating to the cathode, GOs were reduced to RGOs by removing the bonded oxygen groups on GOs, which is consistent with the results reported by Guo et al.[28] This step improves the conductivity of the floating electrodes for the subsequent electrodeposition. (II) RGOs were detached from cathode and transported to the anode by magnetic stirring. (III) At anode and at the current density of 30 mA cm^{-2}, the citrate anions were oxidized to carbonate anions (CO_3^{-2}), which were bonded with Mn^{2+} to form $MnCO_3$ deposits. Surprisingly, these $MnCO_3$ deposits are mesoporous single crystals (Fig. 2). It is believed that the electrodeposition on the floating electrodes is a process of pulse plating that facilitates the formation MSC structure. (IV) In the subsequent floating, RGOs acted as a flexible cloth that wrapped up the deposited $MnCO_3$ MSCs, forming graphene-wrapped $MnCO_3$ MSCs. (V) The whole process continued until the composite material was too heavy to be carried to the Pt and stainless steel electrodes. This DFE method is facile, cost effective and scalable, which is believed to establish a new platform to synthesize various graphene-wrapped composite materials for many applications. It is also noticed that the inclusion of $MnCO_3$ MSCs prevents the restacking of RGOs during GO reduction.[10]

In order to confirm the reactions occurring on Pt and stainless steel electrodes, the same setup was used in a control experiment (Fig. S1), except that the bath was divided into two compartments separated by a filter paper. GOs were added into both parts and stirred by magnetic bars. After electrodeposition at the current densities of 30~70 mA cm^{-2}, GOs were kept intact at the anode, while RGOs were found at the cathode, as characterized by X-ray photoelectron spectroscopy (XPS) in Fig. S1. Most importantly, the formation of $MnCO_3$ or MnO_x particles was not observed in either compartment, implying that $MnCO_3$ in Fig. 1a was deposited on RGOs transported from the cathode (Fig. 1a). In addition, another control experiment (Fig. S2) was conducted in an aqueous electroplating bath of 0.3 M Sodium EDTA and 0.3 M $MnSO_4$. No observation of $MnCO_3$ confirms that it is the citrate anions that were oxidized to carbonate anions (CO_3^{-2}) and bonded with Mn^{2+} to form $MnCO_3$ deposits. The oxidation of citrate anions at anodes have also been reported previously by other researchers.[31]

Structural characterization of graphene-wrapped $MnCO_3$ MSCs

The morphology and microstructure of the composite materials electrodeposited from DFE method shown in Fig. 1a have been carefully characterized. Low-magnification scanning electron microscropy (SEM) image (Fig. 1b, Fig. 1c) shows that the deposited particles are composed of Mn, C and O (Fig. S3a), and have an ellipsoid shape or rice-like shape with the length of ~700 nm and the width of ~250 nm. A thin layer of graphene was found to wrap around the particle (Fig. 1c), forming a graphene-wrapped morphology. In addition, these graphene-wrapped particles are imbedded in the connected graphene matrix (Fig. 1b and Fig. S3), indicating the formation of a 3D, conductive composite structure. In few uncovered areas on the surface of the particle, the high-magnification SEM image (Fig. 1d) reveals a mesoporous structure for the particles, with the pore size being in the range of 5 to 10 nm. A cross-section view of the particles is also shown in Fig. S4, in which a mesoporous structure is clearly observed in the inner part of the particles.

The powder X-ray diffraction (XRD) pattern of the as-deposited composite materials (black spectrum in Fig. 2a) shows that all the sharp peaks can be assigned to the rhombohedral phase of $MnCO_3$ (JCPDS No. 44-1472, the standard spectrum shown as red in Fig. 2a) with the space group of R,-3,c. Although a small bump at small angles can be observed, the characteristic peak of graphene is not clearly identified in the XRD pattern, which may be due to the low concentration of graphene in the composite materials and will be discussed later. The peaks in the XRD pattern are so sharp that the peak widths are much narrower than those for nanocrystalline $MnCO_3$ synthesized before,[15] indicating the large-size and well-crystallized particles formed in this novel DFE method. Interestingly, electron diffraction (Fig. 1c) taken from the complete particle in Fig. 1b produces the Laue diffraction pattern that was indexed to [100] zone axis of Rhombohedral phase of $MnCO_3$, suggesting that the resulted particles are mesoporous single crystals. High-resolution transmission electron microscopy (HRTEM) image in Fig. 2d further confirms that, although each rice-like $MnCO_3$ particle is mesoporous (indicated as white circles), its scaffold as a whole is a single crystal. XPS analyses in Fig. 2e compare C1s spectra

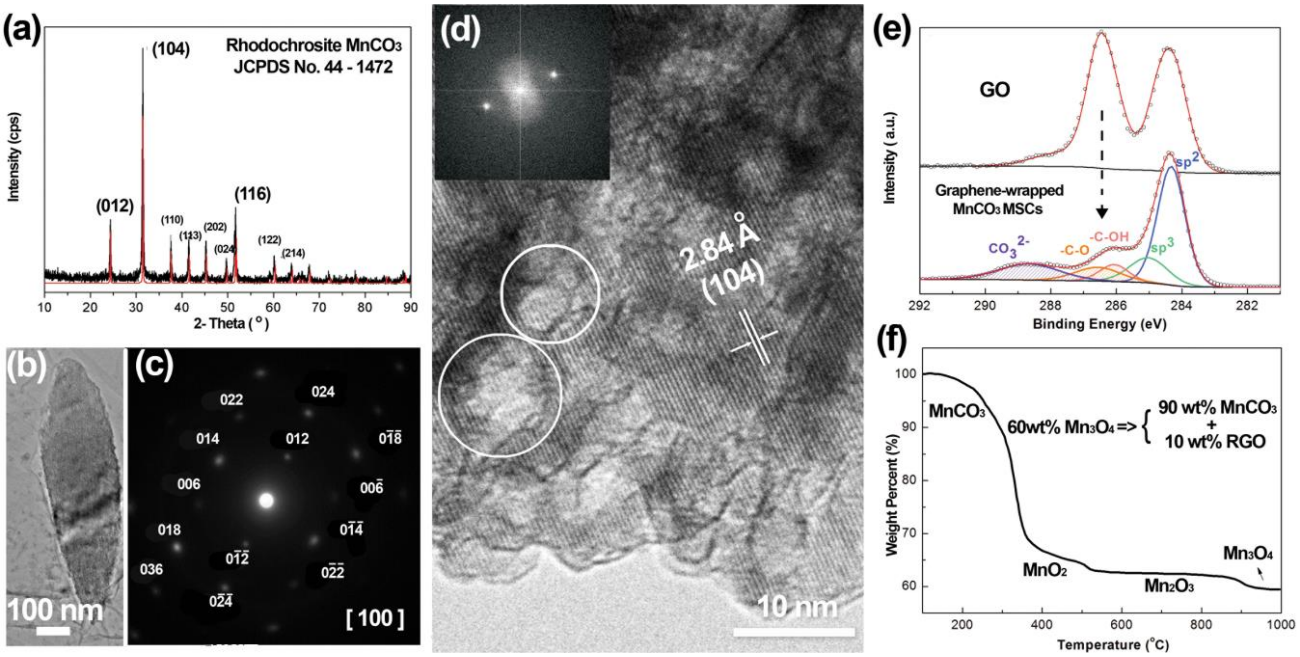

Figure 2. (a) XRD spectrum of graphene-wrapped $MnCO_3$ MSCs, (b) TEM image of graphene-wrapped $MnCO_3$ MSCs. (c) Electron diffraction Laue pattern collected from a complete mesoporous crystal in (b) assigned to rhodochrosite $MnCO_3$ with [100] zone axis. (d) HRTEM image and the inserted fast Fourier transform (FFT). (e) XPS C 1s spectra of as-prepared GOs and graphene-wrapped $MnCO_3$ MSCs. (f) TGA of graphene-wrapped $MnCO_3$ MSCs used for electrochemical measurements.

obtained from GOs (upper spectrum) and the as-deposited composite materials (lower spectrum). The significant decrease of the peaks for the oxygenated groups, as indicated by the dashed arrow in Fig. 2e, suggests the successful reduction of GOs to RGOs during DFE process. Mn 3s spectrum in Fig. S5c shows that Mn ions keep their valence at +2, while O1s spectrum in Fig. S5d implies the presence of CO_3^{-2} anions, both of which suggest the formation of $MnCO_3$ particles in the composite materials. These results agree well with those from SEM, TEM and XRD observations.

Fig. 1 and Fig. 2 reveal that the obtained composite materials from DFE method are submicron, graphene-wrapped $MnCO_3$ MSCs. It is the first time that MSCs were electrodeposited from an aqueous bath in such a low temperature and template-free process. This method also provides a new strategy to synthesize graphene-wrapped composite materials.

Superior electrochemical performance of graphene-wrapped $MnCO_3$ MSCs

The resulting submicron, graphene-wrapped $MnCO_3$ MSCs were used directly as the electrochemically active materials in LIBs. Although nanometer-size active materials have demonstrated improved performance when normalized to the weight of active materials only, these nanomaterials require a high percentage of conductive and binding materials in the electrodes, normally over 20 wt% in total, sacrificing the final performance of the full cell.[32] Their low tap density also results in a low volumetric energy density.[33] In this sense, the structure of submicron, graphene-wrapped MSCs is an ideal structure to be used as active materials in LIBs, since it adopts the advantages of high tap density from microparticles, large tolerance to volume expansion from mesoporosity, and high conductivity from graphene. In addition, high graphene loadings in the composite materials would also reduce their tap density; and hence, the graphene loading in this work was controlled at a low level, 10 wt% of the total composite materials (Fig. 2f). The weight percentage of graphene in graphene-wrapped MnCO3 MSCs was also calculated to be 9.7 wt%, which was made based on the amount of Mn_2O_3 measured at 800°C as shown in Figure 2f. The conductive additive, Super-C65 carbon black, and the binder material, polyvinylidene fluoride, used in this work were kept as low as 6 wt% and 4 wt%, respectively. Accordingly, all the performance data below are normalized against the total weight of graphene and $MnCO_3$ MSCs.

Fig. 3 shows the electrochemical performance of graphene-wrapped $MnCO_3$ MSCs when used as the anode for LIBs. The electrochemical measurements were conducted within the potential range of 0.01~3.0 V and at different current densities ranging from 100 mA g^{-1} to 5,000 mA g^{-1}. As shown in Fig. 3a, there is a long flat potential plateau at ~0.3 V in the first discharging curve at a current density of 100 mA g^{-1}, which offers 1,279 mAh g^{-1} for the initial reduction process. The first charging capacity of 867 mAh g^{-1} was recorded, corresponding to the coulombic efficiency of 67.8%. The low coulombic efficiency in the first cycle was attributed to the formation of solid electrolyte interface (SEI) film on the surface of active particles.[15] In the second cycle, the discharging capacity keeps at a high value of 900 mAh g^{-1} and the coulombic efficiency increases up to 96.7%. During the following cycles, the discharging capacity slowly increases up to 954 mAh g^{-1} at the

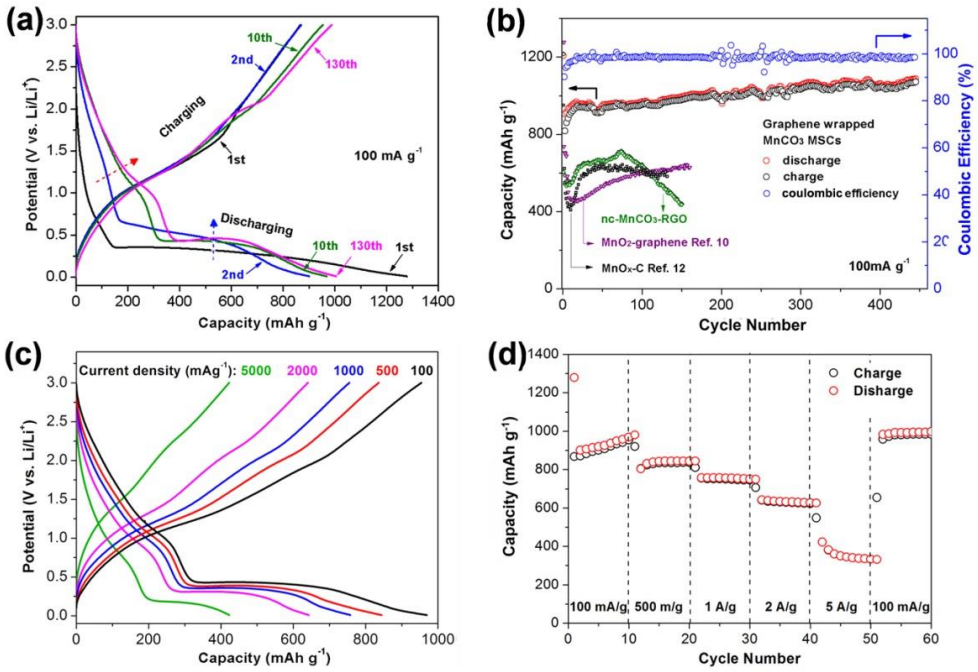

Fig. 3 (a) Charging-discharging curves and (b) cyclability data of graphene-wrapped $MnCO_3$ MSCs within 0.01~3.0 V at 100 mA g^{-1}. (c) Charging-discharging curves and (d) cyclability data of graphene-wrapped $MnCO_3$ at different current densities, ranging from 100 mA g^{-1} to 5,000 mA g^{-1}.

10th cycle and up to 1,000 mAh g^{-1} at the 130th cycles. Accordingly, the coulombic efficiency also increases to over 98% after 10 cycles. The reported discharging capacity in Fig. 3(b) is much higher than the theoretical capacities of both $MnCO_3$ (466 mAh g^{-1})[15] and Graphene (744 mAh g^{-1}),[11] suggesting the high accessibility for lithium insertion and extraction on the graphene-wrapped $MnCO_3$ MSCs. Similar phenomenon has also been found for MnO[11] and MnO_x [12] with the valence of Mn ions smaller than +4. The reason for this high capacity will be discussed later. More interestingly, the graphene-wrapped $MnCO_3$ MSCs deliver the reversible capacity higher than 1,000mAh g^{-1} for over 400 cycles at 100 mA g^{-1} (Fig. 3b).

In addition, high rate capability has also been obtained for the anodes made from graphene-wrapped $MnCO_3$ MSCs. Fig. 3c shows that a reversible capacity of 640 mAh g^{-1} has been reached at a high current density of 2,000 mA g^{-1}. At a current density of 5000 mA g^{-1}, a high capacity of 422 mAh g^{-1} can be delivered. Fig. 3d further shows that the reversible capacity is stable at different current densities ranging from 100 mA g^{-1} to 5,000 mA g^{-1}. Therefore, graphene-wrapped $MnCO_3$ MSCs demonstrate high capacity, high rate capacbility and excellent cycling performance in Fig. 3. To the best of our knowledge, this electrochemical performance are the best results that have been reported for $MnCO_3$ so far, and even better than most of the results reported for MnO_x.[8-10] Although a relatively large potential range, 0.01~3.0 V, was still used in this paper, the shortcoming arising from this large potential range can be compensated by the significantly improved capacity and cycle life shown in Figure 3, demonstrating their practical potential to be used in LIBs. Considering its low cost,[13-15] $MnCO_3$ has been proven to be a new promising candidate as the anode material for LIBs.

Structural advantages from graphene-wrapped $MnCO_3$ MSCs

In order to understand the superior electrochemical performance in Fig. 3 and to elucidate the advantages of the graphene-wrapped MSCs structures, hydrothermal nanocrystalline $MnCO_3$-RGO (nc-$MnCO_3$-RGO)[15] (Fig. S6) and MnO_2 nanoflakes-RGO (nano-MnO_2-RGO)[34] (Fig. S7) composites were synthesized and their electrochemical performance was evaluated. Fig. 4a shows the cyclic voltammetry (CV) curves of graphene-wrapped $MnCO_3$ MSCs in the initial 10 scans within 0.01~3.0 V at a scan rate of 0.02 mV s^{-1}. In the first cycle, a broad reduction peak beginning from 0.44 V and centered at 0.22 V corresponds to the formation of a SEI layer and the complete reduction of Mn^{2+} to Mn^0.[10-12] The main oxidation peak at 1.22 V could be ascribed to the oxidation of Mn^0 to Mn^{2+} in the cathodic process.[10-12,35] During the second cycle, the intensity of the main reduction peak decreases and shifts significantly up to 0.43 V. In the reversed scan of the second cycle, a new oxidation peak at 1.85 V starts to appear and gets stronger and stronger in the following cycles. At the fifth cycle, another broad oxidation peak at a higher potential of 2.30 V appears. In accordance with two new oxidation peaks, a new reduction peak at 1.06 V becomes evident gradually after the second cycle. The new oxidation peaks at potentials higher than 1.22 V reveal that new oxidation reactions were occurring in the system. It is suggested that Mn^{2+} has been further oxidized to higher oxidation states.[11,12] To clarify this point, charging discharging curves at the 10th cycle for the samples of nano-MnO_2-RGO (with Mn^{4+}) were obtained, which were compared with those for graphene-wrapped $MnCO_3$ MSCs (with Mn^{2+}) in Fig. 4b. It

shows that both samples demonstrate similar charge discharge curves at the 10th cycle, especially the appearance of the potential plateau at 1.0 V in the discharging curves. In addition, both samples demonstrate a potential plateau at around 1.85 V in the charging curves, which is consistent with the CV curves in Figure 4a. Although this new potential plateau for graphene-wrapped MnCO3 MSCs is not as obvious as that for nano-MnO2-RGO in Figure 4b, it gets stronger and stronger in the following cycles, which can be seen from the charging curve after 130 cycles in Figure 3a. It indicates that the redox reactions for graphene-wrapped $MnCO_3$ MSCs in the potential range higher than 1.0 V is the reversible reactions between Mn^{2+} and high oxidation state Mn associated with lithium-ion extraction and insertion. Similar phenomenon has also been found for MnO/graphene and MnO_x/carbon electrodes with the valence of Mn ions smaller than +4.[11,12] It is noted that the reported discharging capacity higher than the theoretical capacity of $MnCO_3$ in Fig. 3b can be attributed to the new oxidation reactions occurred in the system, which is suggested to be the further oxidation of Mn^{2+} to higher oxidation state.

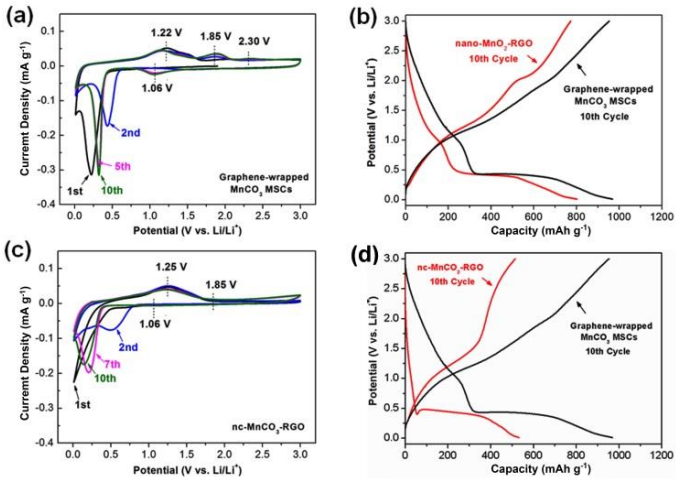

Fig. 4 (a) Cyclic voltammetry measurements of graphene-wrapped $MnCO_3$ MSCs. (b) Comparison of charging-discharging curves between graphene-wrapped $MnCO_3$ MSCs and nano-MnO_2-RGO at the 10th cycle. (c) Cyclic voltammetry measurements of nc-$MnCO_3$-RGO. (d) Comparison of charging-discharging curves between graphene-wrapped $MnCO_3$ MSCs and nc-$MnCO_3$-RGO at the 10th cycle.

In contrast to the CV curves of graphene-wrapped $MnCO_3$ MSCs (Fig. 4a), CV curves in Fig. 4c shows that Mn^{2+} in nc-$MnCO_3$-RGO could not be re-oxidized to higher oxidation states in the initial 10 cycles. Accordingly, the discharging curve of nc-$MnCO_3$-RGO at the 10th cycle (Fig. 4d and Fig. S8a) did not demonstrate a clear potential plateau at 1.0 V, which is in agreement with the CV curves in Fig. 4c. Hence, nc-$MnCO_3$-RGO in Fig. 4d demonstrates a low reversible capacity of 582 mAh g^{-1} within 0.01~3.0 V.

Comparing Fig. 4a with Fig. 4c, it is interesting to see that the initial microstructure of the active particle (i.e., precursor

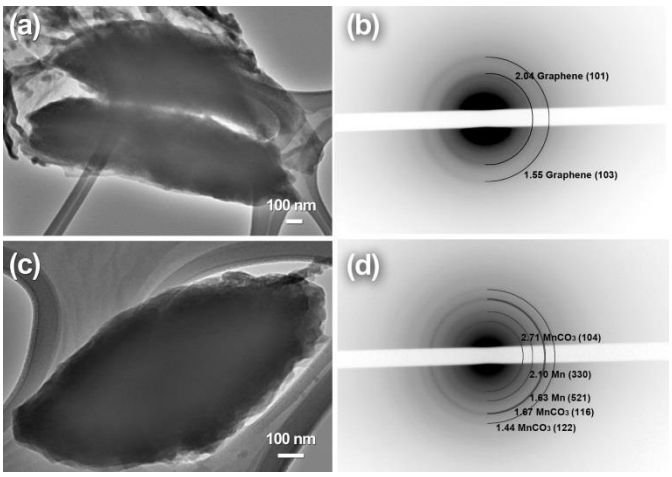

Fig. 5 (a) TEM and (b) selected-area diffraction of graphene-wrapped $MnCO_3$ MSCs after 10 cycles. (c) TEM and (d) selected-area diffraction of nc-$MnCO_3$-RGO after 10 cycles.

particles) significantly affects their electrochemical performance. Poizot et al. also found that the morphology of the precursor particles, e.g., the particle size of metal oxides, affects the state of division of the conversion reaction products, and hence the electrochemical performance.[17] In order to further illustrate how the microstructure of the precursor particles affects their electrochemical performance, the cycled graphene-wrapped $MnCO_3$ MSCs and nc-$MnCO_3$-RGO samples were investigated by TEM and selected-area diffraction. Fig. 5a and Fig. 5b show that, after 10 cycles, the single crystal structure of $MnCO_3$ has been evolved to the amorphous structure. In Fig. 3a, it has been shown that the new potential plateau at 1.0 V in the discharging curves becomes more and more pronounced (dashed red arrow in Fig. 3a, and the over-potential decreases for the conversion reaction at potentials lower than 0.5 V (dashed blue arrow in Fig. 3a), after cycling. It is, therefore, concluded that the evolution of microstructure from single crystals to the amorphous structures lowers the over-potential of the conversion reaction and actives the new reversible reactions at potentials higher than 1.0 V. Maier and coworkers reported that amorphization of crystalline RuO_2 could enhance the lithiation potential (i.e., lower the over-potential of lithiation) owing to the enhanced Gibbs free energy compared with the crystalline bulk RuO_2.[36] It is also reported that amorphous structure of manganese oxide effectively lowers the resistance for the conversion reaction.[12] These are consistent with the conclusion obtained in Fig. 5a and Fig. 5b. On the contrary, $MnCO_3$ in nc-$MnCO_3$-RGO keeps nanocrystalline structure after 10 cycles (Fig. 5c and Fig. 5d) and the new potential plateau at 1.0 V has not been activated after 10 cycles. It further proves that it is the evolution of microstructure from single crystals to the amorphous structures that actives the new reversible reactions. It also implies that nanocrystalline $MnCO_3$ is more difficult to be transformed to the amorphous structure after cycling; and hence, the discharging capacity is lower for nc-$MnCO_3$-RGO than that for graphene-wrapped $MnCO_3$ MSCs. It is suggested that the lithiation of nanocrystalline $MnCO_3$ starts

from their grain boundaries. This first-step lithiation exposes fresh surfaces to the electrolyte and forms additional SEI films, which, in turn, retards further lithiation of inner part of $MnCO_3$.

The ease of the transformation from single crystals to the amorphous structure lowers the over-potential of the conversion reaction and actives the new reversible reactions at potentials higher than 1.0 V, leading to the high capacities presented in Fig. 3a. In addition, the phase transformation during cycling causes the loss of electrical contact for the active materials,[11,12,15] which can be minimized by the graphene-wrapped morphology (Fig. 3b).[10] As shown in Fig. S9, graphene-wrapped morphology has been retained after cycling. This phase transformation also induces large volume change,[11,12,15] which can be accommodated by the mesoporous structure of the precursor particles. As a result, graphene-wrapped mesoporous structure demonstrates the cycling performance superior to nc-$MnCO_3$-RGO (Fig. 3b). Furthermore, the high conductivity shell provided by the graphene-wrapped morphology can be attributed to the high rate capability presented in Fig. 3c and Fig. 3d. Therefore, it is the designed structure, graphene-wrapped MSCs, of $MnCO_3$ that is attributed to the superior electrochemical performance presented in Fig. 3.

Conclusions

In conclusions, a unique structure of graphene-wrapped mesoporous single crystals was designed and applied on low-cost $MnCO_3$ for lithium-ion storage. In order to synthesize this unique structure, we, for the first time, reported a low-temperature (70°C) and template-free electrodeposition method, referred to as dynamic floating electrodeposition. During DFE process, graphene oxides were dynamically floating between two electrodes, which were first reduced at cathode, transported to anode for the deposition of $MnCO_3$ MSCs, and wrapped up in the subsequent floating. This DFE method is facile, cost effective and scalable, which is believed to establish a new platform to synthesize various graphene-wrapped composite materials for many applications. The resulting submicron, graphene-wrapped $MnCO_3$ MSCs reached a high reversible capacity of 900 mAh g^{-1} after the initial cycle and delivered over 1,000 mAh g^{-1} after 130 cycles. In addition, the reversible capacity kept at this high level for more than 400 cycles, and maintained 422 mAh g^{-1} at a high rate of 5,000 mA g^{-1}. It is also the first time that this high performance has been achieved on $MnCO_3$ for lithium-ion storage. Furthermore, the superior electrochemical performance was found to be highly related to the designed novel structure. The graphene-wrapped $MnCO_3$ MSCs are able to deliver high capacities because of the easy transformation from single crystal structure to the amorphous structure during cycling, and exhibit the high cyclability because of the graphene-wrapped morphology. The insightful gains from this work, such as the structural design of the active materials, the DFE synthesis method and the high performance for lithium-ion storage, provide new avenues to the future development of high performance energy storage systems.

Acknowledgements

The authors would like to thank the Natural Sciences and Engineering Research Council (NSERC) of Canada for financial support.

Notes and references

§ M. Gao and X. Cui contribute equally to this work

1 Y. M. Lin, P. R. Abel, A.Heller, C. B. Mullins, *J. Phys. Chem. Lett*., 2011, **2**, 2885-2891.
2 X. Jia, Z. Chen, X. Cui, Y. Peng, X. Wang, G. Wang, F. Wei, Y. Lu, *ACS Nano*, 2012, **6**, 9911-9919.
3 Z. S. Wu, W. Ren, L. Wen, L. Gao, J. Zhao, Z. Chen, G. Zhou,F. Li, H. M. Cheng, *ACS Nano*, 2010, **4**, 3187-3194.
4 J. S. Chen, T. Zhu, Q. H. Hu, J. Gao, F. Su, S. J. Qiao, X. W. Lou, *ACS Appl. Mater. Interfaces*, 2010, **2**, 3628-3635.
5 Y. S. Lin, J. G. Duh, M. H. Hung, *J. Phys. Chem. C,* 2010, **14**, 13136-13141.
6 J. Lin, Z. Peng, X. Xiang, G. Ruan, Z. Yan, D. Natelson, J. M. Tour, *ACS Nano*, 2013, **7**, 6001-6006.
7 X. Zhou, L. J. Wan, Y. G. Guo, *Adv. Mater*., 2013, **25**, 2152-2157.
8 H. Xia, M. Lai, L. Lu, *J. Mater. Chem*., 2010, **20**, 6896-6902.
9 A. L. M. Reddy, M. M. Shaijumon, S. R. Gowda, P. M. Ajayan, *Nano Lett.* 2009, **9**, 1002-1006.
10 L. Li, A. R. O. Raji, J. M.Tour, *Adv. Mater*., 2013, **25**, 6298-6302.
11 Y. Sun, X. Hu, W. Luo, F. Xia, Y. Huang, *Adv. Funct. Mater*., 2013, **23**, 2436-2444.
12 J. Guo, Q. Liu, C. Wang, M. R. Zachariah, *Adv. Funct. Mater*., 2012, **22**, 803-811.
13 S. Lei, Z. Liang, L. Zhou, K. Tang, *Materials Chemistry and Physics*, 2009, **113**, 445-450.
14 M. Zheng, H. Zhang, X. Gong, R. Xu, Y. Xiao, H. Dong, X. Liu, Y. Liu, *Nanoscale Research Letters*, 2013, **8**, 166.
15 Y. Yan, Y. Zhu, Y. Yu, J. Li, T. Mei, Z. Zhu, Y. Qian, *J. Nanosci. Nanotechnol*., 2012, **12**, 7334-7338.
16 S. Devaraj, H. Y. Liu, P. Balaya, *J. Mater. Chem. A*., 2014, **2**, 4276-4281.
17 P. Poizot, S. Laruelle, S. Grugeon, L. Dupont, J-M. Tarascon, *Nature*., 2000, **407**, 496-499.
18 E. J. W. Crossland, N. Noel, V. Sivaram, T. Leijtens, J. A. Alexander-Webber, Snaith, H. J. *Nature*, 2013, **495**, 215-219.
19 D. Su, S. Dou, G. Wang, *Nano Res*., 2014, **7**, 794-803.
20 D. Su, M. Ford, G. Wang, Sci Rep., 2012, **2**, 924.
21 J. Weickert, R. B. Dunbar, H. C. Hesse, W. Wiedemann, L. Schmidt-Mende, *Adv. Mater*., 2011, **23**, 1810-1828.
22 C. Dickinson, W. Zhou, R. P. Hodgkins, Y. Shi, D. Zhao, H. He, *Chem. Mater*., 2006, **18,** 3088-3095.
23 P. Yang, D. Zhao, D. I. Margolese, B. F. Chmelka, G. D. Stucky, *Nature*, 1998, **396**, 152-155.
24 K. Jiao, B. Zhang, B. Yue, Y. Ren, S. Liu, S. Yan, C. Dickinson, W. Zhou, H. He, *Chem. Commun*., 2005, 45, 5618-5620.
25 H. Wang, Y. Yang, Y. Liang, J. T. Robinson, Y. Li, A. Jackson, Y. Cui, H. Dai, *Nano Lett*. 2011, **11**, 2644-2647.
26 C. Y. Su, A. Y. Lu, Y. Xu, F. R. Chen, A. N. Khlobystov, L. J. Li, *ACS Nano,* 2011, **5**, 2332-2339.
27 X. Xu, D. Huang, H. Cao, M. Wang, S. M. Zakeeruddin, M. Gratzel, *Sci Rep*., 2013, 3, 1489.
28 H. L. Guo, X. F. Wang, Q. Y. Qian, F. B. Wang, X. H. Xia, *ACS Nano*, 2009, **9**, 2653-2659.

29 W. S. Hummers Jr, R. E. Offeman, *J. Am. Chem. Soc*., 1958, **80**, 1339-1339.
30 T. Chen, B. Zeng, J. L. Liu, J. H. Dong, X. Q. Liu, Z. Wu, X. Z. Yang, Z. M. Li, *J. Phys. Conf. Ser*., 2009, 188, 012051.
31 G. Trettenhahn, A. Koberl, *Electrochimica Acta*., 2007, **52**, 2716-2722.
32 X. Cui, J. Chen, T. Wang, W. Chen, *Sci Rep*., 2014, 4, 5310.
33 Y. Deng, Y. Zhou, Z. Shi, X. Zhou, X. Quan, G. Chen, *J. Mater. Chem. A,* 2013, **1**, 8170-8177.
34 J. Qu, L. Shi, C. He, F. Gao, B. Li, Q. Zhou, H. Hu, G. Shao, X. Wang, J. Qiu, *Carbon*, 2014, **66**, 485-492.
35 H. Wang, L. Cui, Y. Yang, H. S. Casalongue, J. T. Robinson, Y. Liang, Y. Cui, H. Dai, *J. Am. Chem. Soc.*, 2010, **132**, 13978-13980.
36 O. Delmer, P. Balaya, L. Kienle, J. Maier, *Adv. Mater*., 2008, **20**, 501-505.

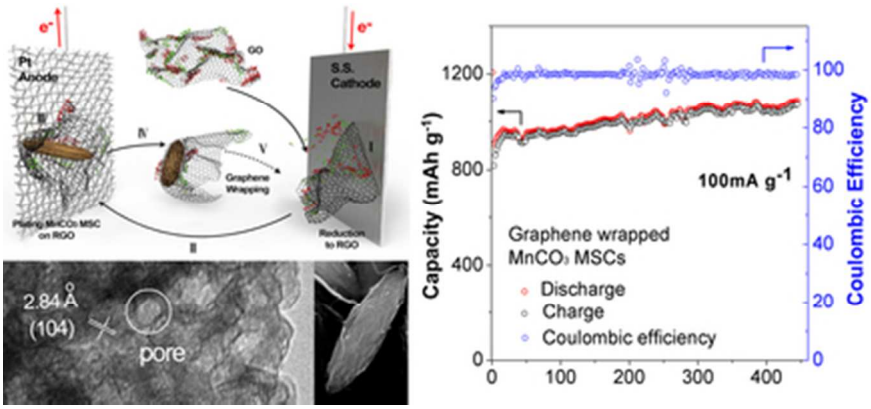

Graphene-wrapped MnCO3 MSCs, synthesized through dynamic floating electrodeposition, demonstrate high capacity (1087 mAh/g) and excellent cycling performance (>400 cycles).
36x16mm (300 x 300 DPI)